

Improving Backscatter Intensity Calibration for Multispectral LiDAR

Shuo Shi, Shalei Song, Wei Gong, Lin Du, Bo Zhu, and Xin Huang, *Senior Member, IEEE*

Abstract—A wavelength-dependent light detection and ranging (LiDAR) backscatter intensity calibration method was developed to maximize the advantages of a multispectral LiDAR system. We established a spectral ratio calibration method for multispectral LiDAR and investigated the effective calibration procedure for the mixed measurement of the effect of incident angle and surface roughness. Experiment results showed that the proposed LiDAR spectral ratio is insensitive to sensor-related factors and advantageous in calibrating the effect of incidence angle and surface roughness. As the product of the LiDAR calibration procedure based on spectral ratio, extended vegetation indexes significantly improve the classification accuracy.

Index Terms—Calibration, light detection and ranging (LiDAR) spectral ratio, multispectral LiDAR, remote sensing, vegetation index.

I. INTRODUCTION

LIGHT detection and ranging (LiDAR) has been widely used to obtain surface geometry and to perform target characterization. LiDAR echo measurement generates a point cloud that represents the coordinates (x, y, z) of the object and is frequently tagged with auxiliary variables. For each point, the intensity (I) value is also simultaneously recorded. An improved automation of the classification and interpretation of laser scanning data has thus become necessary. The use of laser backscatter intensity data has led to improvements in the development of automatic methods for tree species determination, canopy structure analysis [1], and fractional cover measurement [2].

A wide range of LiDAR sensors that use multiple laser wavelengths have been developed to further investigate the potential of laser backscatter intensity. Among these new LiDAR sensors, the concept of multispectral (or hyperspectral) LiDAR can produce one-shot topographic and multispectral intensity information. A number of prototypes of multispectral LiDAR

Manuscript received October 23, 2014; revised January 23, 2015 and February 13, 2015; accepted February 17, 2015. Date of publication March 3, 2015; date of current version March 24, 2015. This work was supported in part by the National Natural Science Foundation of China under Grant 41101334 and Grant 41127901, by the 973 Program under Grant 2011CB707106, and by the Chenguang Project of Wuhan under Grant 2014070404010229.

S. Shi, W. Gong, L. Du, B. Zhu, and X. Huang are with the State Key Laboratory of Information Engineering in Surveying, Mapping, and Remote Sensing, Wuhan University, Wuhan 430079, China, and also with the Collaborative Innovation Center for Geospatial Technology, Wuhan 430079, China.

S. Song is with the Wuhan Institute of Physics and Mathematics, Chinese Academy of Sciences, Wuhan 430071, China.

Color versions of one or more of the figures in this paper are available online at <http://ieeexplore.ieee.org>.

Digital Object Identifier 10.1109/LGRS.2015.2405573

systems, which are mainly laboratory based, have been developed [3]–[5]. The detection results of multispectral LiDAR include point cloud and multispectral intensities: $[x, y, z, I(\lambda)]$, where $I(\lambda)$ is the backscattered intensity, and I is a function of laser wavelength λ . The selected laser wavelength λ leads to a certain wavelength-dependent backscatter characteristic of the sensed surface.

The great potential of multispectral LiDAR is based on the differences in backscatter intensities at multiple wavelengths. Backscatter intensity calibration is essential in studying the characteristics of the sensed targets. Backscatter signals are mainly affected by several factors, including instrumental and atmospheric effects, target scattering characteristics, and measurement geometry [6]–[8]. Studies have focused on correction techniques for adjusting the intensity variations of single-wavelength LiDAR systems and have subsequently demonstrated the availability of such correction methods [9]–[11]. However, calibration procedures are usually complex and restricted to some extent, and they contain complex parameters. Calibration for multispectral LiDAR is particularly difficult, because of the increase in the number of wavelengths. The same is particularly true if a single-wavelength calibration method is employed.

In the present study, we maximize the advantages of multispectral LiDAR in terms of backscatter intensity calibration. We develop a laboratory-based prototype of a multispectral LiDAR [5] designed for vegetation applications. This system is designed to take measurements at four wavelengths (556, 670, 700, and 780 nm). Our study used data from this multispectral LiDAR. Specifically, we aim to achieve the following objectives:

- 1) to establish multispectral intensity calibration methods based on the radar equation;
- 2) to evaluate the capability for improvement of a calibration method for multispectral LiDAR;
- 3) to study the effect of calibration on target classification, given the necessity of conducting further investigations on any possible intensity influencing factors of multispectral LiDAR detection.

II. PHYSICAL BACKGROUND OF MULTISPECTRAL LiDAR CALIBRATION

A. Radar Equation

This section concisely presents the physical basis of the radiometric calibration of multispectral LiDAR intensity. The radar equation, which has been applied in laser scanning, defines received power as a function of sensor parameters. The equation

defines the power that enters the LiDAR receiver as follows [6], [7]:

$$P_r = \frac{P_t D_r^2}{4\pi R^4 \beta_t^2} \eta_{\text{sys}} \eta_{\text{atm}} \sigma \quad (1)$$

where the received signal power P_r is a function of the transmitted signal power P_t , the receiver aperture diameter D_r , the range from the sensor to the target R , the laser beam width β_t , the system transmission factor η_{sys} , the atmospheric transmission factor η_{atm} , and the target cross section σ [7].

The so-called backscatter cross section σ is the parameter related to the backscattering characteristics of a target [6]. All target parameters can be explained as follows:

$$\sigma = \frac{4\pi}{\Omega} \rho A_S \quad (2)$$

where the target cross section σ is a function of the scattering solid angle of the target Ω , the target reflectance ρ , and the target area A_S . Reflectance is the portion reflected to the incident radiation from the target area in the laser wavelength. This value is averaged over the total target area.

The reflectance of target ρ can be obtained as follows according to (1) and (2):

$$\rho = \frac{P_r R^4 \beta_t^2 \Omega}{P_t D_r^2 A_S \eta_{\text{sys}} \eta_{\text{atm}}}. \quad (3)$$

This function is based on the radar equation. The intensity measured by the LiDAR system can be used to calculate the target reflectance and to obtain the characteristics of the target.

B. Backscattering Characteristics of Multispectral LiDAR

Our study involves data from a multispectral LiDAR system that is designed for vegetation applications [5]. The principle of this multispectral LiDAR has been well established in the application of object identification and observation, particularly in the monitoring of the growth and nutrition status of vegetation. The operation of the multispectral LiDAR system is presented as a block diagram in Fig. 1. Four laser wavelengths (556, 670, 700, and 780 nm) are selected for the detection of leaf nitrogen and chlorophyll content [12]. These four laser diodes are synthesized into a beam. An independent laser range sensor performs range measurements. The synthesized backscatter signals are received by the Schmidt–Cassegrain telescope and divided into four channels for photomultiplier detection. The backscatter intensities and range of the objects can then be obtained through data acquisition and the processing of the subsystem in a computer. All the transmitting and receiving facilities of the LiDAR system are fixed on a motorized precision stage to ensure scanning detection and synchronous signal reception. Through laser scanning and ranging, point cloud comprising probe points with geometric information (x, y, z) and intensity (I) can be obtained.

The LiDAR equation defines target reflectance as a function of received power and sensor parameters. This equation can also be applied for the multispectral LiDAR system. According

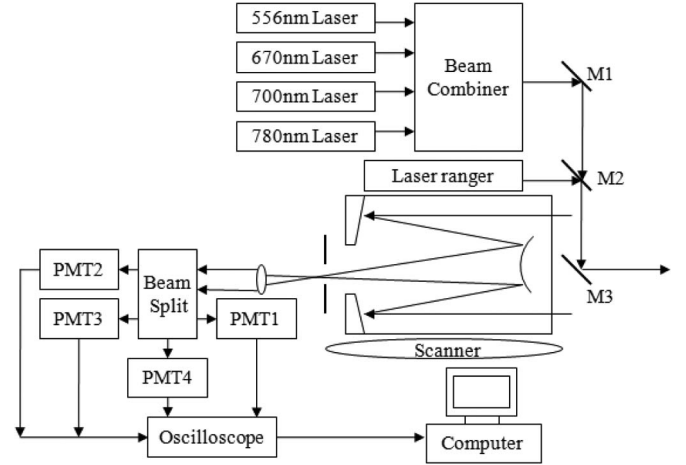


Fig. 1. Block diagram of multispectral LiDAR.

to (3), wavelength-dependent reflectance can be expressed as follows:

$$\rho_{\lambda_i} = \frac{P_{r_{\lambda_i}} R^4 \beta_{t_{\lambda_i}}^2 \Omega_{\lambda_i}}{P_{t_{\lambda_i}} D_r^2 A_{S_{\lambda_i}} \eta_{\text{sys}_{\lambda_i}} \eta_{\text{atm}_{\lambda_i}}} \quad (4)$$

where i is the laser wavelength of the multispectral LiDAR. With the increase in the number of wavelengths, additional information about the target features can be obtained. Owing to the advantage of multiwavelength backscatter intensities, the calibration of the local incidence angle and surface roughness of the target becomes easy and efficient. The practical procedure is explained in detail in Section III.

III. METHOD

This study proposed a calibration method based on spectral ratio with consideration of the advantage of multispectral signals. In addition, vegetation indexes that could help improve the capability of object classification were established as products of the calibration method.

A. LiDAR Spectral Ratio Calibration Method

The emissions of four lasers were strictly synchronized and combined into a beam to ensure that the near and far fields of light overlap. This procedure causes the influences of the incidence angle and sensor factors within the footprint to become similar at each laser wavelength. Thus, the calculation of spectral ratios should be insensitive to sensor-related factors and be influenced primarily by the target characteristics.

According to (4), the wavelength-dependent laser spectral ratio is calculated as follows:

$$\frac{\rho_{\lambda_1}}{\rho_{\lambda_2}} = \frac{P_{r_{\lambda_1}} \beta_{t_{\lambda_1}}^2 \Omega_{\lambda_1}}{P_{t_{\lambda_1}} A_{S_{\lambda_1}} \eta_{\text{sys}_{\lambda_1}} \eta_{\text{atm}_{\lambda_1}}} \cdot \frac{P_{t_{\lambda_2}} A_{S_{\lambda_2}} \eta_{\text{sys}_{\lambda_2}} \eta_{\text{atm}_{\lambda_2}}}{P_{r_{\lambda_2}} \beta_{t_{\lambda_2}}^2 \Omega_{\lambda_2}}. \quad (5)$$

Assuming that the beams were perfectly aligned, the influence of the incidence angle, area of the target within the footprint, and so on, would be similar at both wavelengths. Thus, the resulting ratio should be insensitive to these factors, which could be removed along with the spectral ratio [13]. Thus, the

reflectance ratio of different wavelengths can be expressed as follows:

$$\frac{\rho_{\lambda 1}}{\rho_{\lambda 2}} = \frac{P_{r_{\lambda 1}}}{P_{r_{\lambda 2}}} \cdot \frac{P_{t_{\lambda 2}} \eta_{\text{sys}_{\lambda 2}} \eta_{\text{atm}_{\lambda 2}}}{P_{t_{\lambda 1}} \eta_{\text{sys}_{\lambda 1}} \eta_{\text{atm}_{\lambda 1}}}. \quad (6)$$

The spectral ratio based on multispectral LiDAR is advantageous in eliminating common sensor factors that are independent of laser wavelengths. Thus, we only need to consider the variations of transmitted signal power P_t , system transmission factor η_{sys} , and atmospheric transmission factor η_{atm} in calculating the LiDAR spectral ratio. All the factors of the LiDAR spectral ratio can be attributed to the following new variable:

$$C_{\text{cal}_{\lambda_i}} = P_{t_{\lambda_i}} \eta_{\text{sys}_{\lambda_i}} \eta_{\text{atm}_{\lambda_i}} \quad (7)$$

where C_{cal} is a calibration constant. We assumed that the laser pulse power and constant atmospheric conditions were highly stable throughout the acquisition process. Thus, we obtained the following simplified equation:

$$\frac{\rho_{\lambda 1}}{\rho_{\lambda 2}} = \frac{P_{r_{\lambda 1}}}{P_{r_{\lambda 2}}} \cdot \frac{C_{\text{cal}_{\lambda 2}}}{C_{\text{cal}_{\lambda 1}}}. \quad (8)$$

The LiDAR spectral ratio of the target was then decomposed into two ratios, namely, the receiving power and the calibration constant ratios, depending on laser wavelengths and the reflectance of the reference surface. The calibration of C_{cal} used in this study was developed for discrete-return multispectral LiDAR intensity based on precalibrated in situ reference targets within the field of view of a laser scanner [8]. In practice, the received intensity at each laser wavelength as shown in (4) is collected using a 99% standard white board (Labsphere Inc.) as a reference target. The backscatter intensities are normalized with the intensity of the Spectralon echo at the same distance. This process produces multispectral backscattered reflectance, which was used in the present study as a calibration parameter.

With the given reference targets, the backscattered reflectance of the target followed the principle in (8). The ratio of the calibration constant can be expressed as

$$\frac{C_{\text{cal}_{\lambda 2}}}{C_{\text{cal}_{\lambda 1}}} = \frac{P_{r_{\text{ref}_{\lambda 2}}}}{P_{r_{\text{ref}_{\lambda 1}}}} \cdot \frac{\rho_{\text{ref}_{\lambda 1}}}{\rho_{\text{ref}_{\lambda 2}}}. \quad (9)$$

The spectral ratio of the measured target can be determined once the ratio of the calibration constant is derived by the calibrated target.

B. Vegetation Index Extended by Spectral Ratio

By establishing a LiDAR calibration procedure based on spectral ratio, multispectral LiDAR offers a unique advantage in eliminating relevant parameters required in radar equation. This advantage helps simplify the calibration procedure and improve calibration accuracy. In addition to the calibration method, LiDAR spectral ratios at multiwavelengths can be employed to establish vegetation indexes.

Since the 1960s, vegetation indexes have been widely used to extract and model various vegetation biophysical variables by remote sensing data [14]. Multispectral LiDAR is now considered as a new approach for measuring vegetation indexes [13], [15]. After the calibration procedure, spectral ratio could be

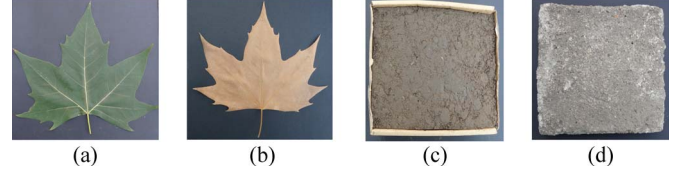


Fig. 2. Four representative measurement targets with various degrees of surface roughness: (a) green leaf of *Platanus orientalis*, (b) deciduous leaf of *P. orientalis*, (c) soil, and (d) cement.

directly extended to all kinds of vegetation indexes for different applications. The spectral ratios developed in the present study can calculate many vegetation indexes for various applications with the multispectral LiDAR.

In particular, the wavelengths at 670 and 780 nm make up the commonly used normalized difference vegetation index (NDVI), which is as follows [14]:

$$\text{NDVI}_{\text{laser}} = \frac{(\rho_{780} - \rho_{670})}{(\rho_{780} + \rho_{670})}. \quad (10)$$

The wavelengths at 556 and 780 nm make up the green NDVI (GNDVI), whose dynamic range is wider than that of the NDVI and whose sensitivity to chlorophyll a concentration is five times greater than that of the NDVI [16]. Thus

$$\text{GNDVI}_{\text{laser}} = \frac{(\rho_{780} - \rho_{556})}{(\rho_{780} + \rho_{556})}. \quad (11)$$

The wavelengths at 670 and 700 nm make up the simple ratio pigment index (SRPI), which is used in the remote estimation of the concentrations of chlorophyll a, chlorophyll b, and carotenoids in soybean leaves [17]. Thus

$$\text{SRPI}_{\text{laser}} = \frac{\rho_{700}}{\rho_{670}}. \quad (12)$$

IV. EXPERIMENT AND DISCUSSION

Laboratory measurements were performed to investigate the effectiveness of the multispectral LiDAR calibration procedure in the mixed backscatter intensity measurement of the incidence angle effect, as well as the surface roughness of the target. The calibration result was evaluated through a classification experiment.

A. Calibration of Incidence Angle and Roughness Effects

Four kinds of objects, namely, healthy leaves of *Platanus orientalis*, deciduous leaves of *P. orientalis*, soil, and cement (see Fig. 2), were selected to represent various degrees of surface roughness. The instrument with four wavelengths was assumed to be effective in discriminating the different objects. All operations were conducted in a darkroom to reduce the influence of the environment factors. The multispectral laser light was horizontally transmitted toward the objects at a distance of 10 m. The measurements of the four targets were taken with an incidence angle ranging from 0° to 80° to evaluate the influence of the incidence angle.

The intensity detection results of the multispectral LiDAR with the influence of the incidence angle are provided in Fig. 3.

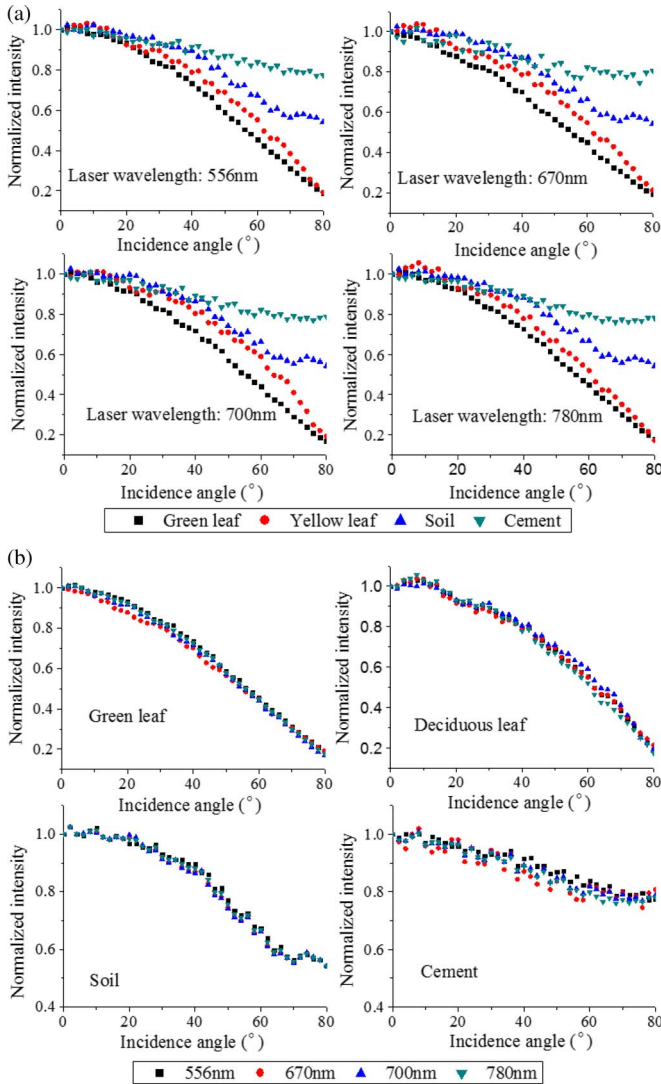


Fig. 3. Multispectral LiDAR intensity versus incidence angle of the four representative targets. The intensity is normalized to 1° at 0°.

Each target exhibited a distinct response according to different laser wavelengths [see Fig. 3(a)]. The four laser wavelengths of each target appeared to exhibit significant correlation [see Fig. 3(b)]. This correlation indicated that the influence of the incidence angle would be similar at both wavelengths. The results provide important evidence that the calibration procedure based on spectral ratio eliminates the incidence angle effect of multispectral LiDAR.

The incidence angles demonstrated similar effects at different wavelengths. Thus, multispectral LiDAR can calibrate this effect with LiDAR spectral ratio based on laser wavelengths. The results of this calibration procedure at wavelengths of 670 and 780 nm are shown in Fig. 4. With the increase of the incidence angle, the value of LiDAR spectral ratio showed small fluctuations compared with the intensity (see Fig. 3). This result revealed the effectiveness of the LiDAR calibration procedure based on spectral ratio in calibrating the incidence angle effect.

Aside from the incidence angle effect, Fig. 3(b) shows the variation in intensity resulting from the surface roughness of the different objects. The green leaf and deciduous leaf both

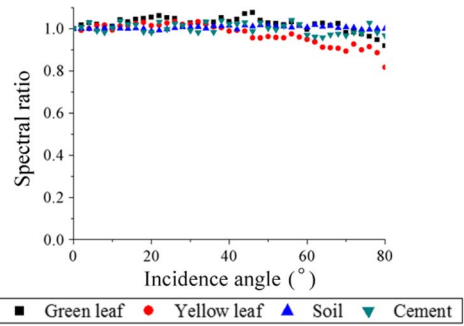


Fig. 4. Effect of incidence angle on I_{780}/I_{670} .

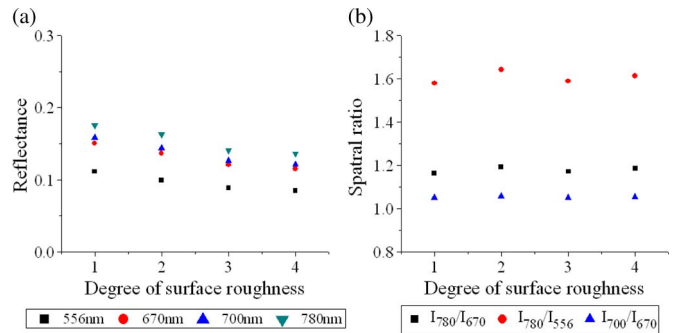


Fig. 5. (a) Reflectance of the four wavelengths of soils with four degrees of surface roughness. The MAREs are 9.70%, 9.95%, 9.97%, and 9.97%. (b) Spectral ratios of the four degrees of surface roughness. The MAREs are 0.94%, 1.37%, and 0.24%.

featured a flat leaf surface and thus had similar smooth curves. Meanwhile, the curves of soil and cement exhibited an irregularity as a result of surface roughness. To evaluate the exact effects of surface roughness, we performed an experiment on a specific object that involved detecting the laser backscatter reflectance of the four different degrees of soil roughness [see Fig. 5(a)]. The roughness increased from degree 1 to degree 4, which means from flat to fragments with no regular shapes. Wavelength dependence was found to be consistent regardless of the surface roughness. The advantage of the spectral ratio method in calibrating the effect of surface roughness is shown in Fig. 5(b). Mean absolute relative error (MARE) was used to indicate the exact effects of surface roughness. The MARE values of the spectral ratios were significantly smaller than that of the single-wavelength reflectance for different degrees of surface roughness.

B. Classification Using Calibrated Vegetation Indexes

The results of the calibration of the incidence angle effect using the LiDAR calibration procedure based on spectral ratio highlight the obvious advantage of multispectral LiDAR. To fully understand the calibration effect, we further classified the four representative objects shown in Fig. 2.

A scanning measurement was performed on the four objects. As shown in Fig. 4, the calibration procedure based on spectral ratio could not easily discriminate the four representative objects, whose responses were similar to I_{780}/I_{670} . However, the vegetation index, as a product of the LiDAR calibration

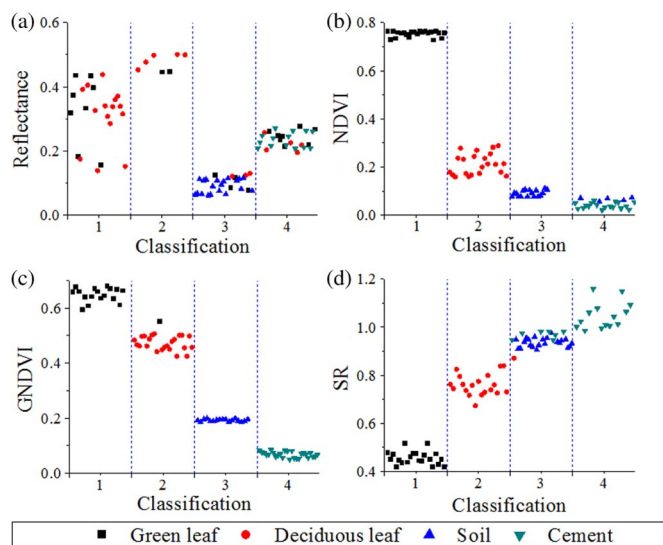


Fig. 6. Classification distribution for the representative objects through the support vector machine approach: (a) 780 nm, classification accuracy is 55.9%; (b) $NDVI_{laser}$, (c) $GNDVI_{laser}$, and (d) $SRPI_{laser}$. The classification accuracy values of the three vegetation indexes are 94%, 98%, and 90%.

procedure based on spectral ratio, could improve the classification accuracy.

To determine whether the vegetation indexes derived from the calibrated laser backscatter intensity are reliable for identifying different objects, we compared the classification results of the 780-nm backscatter intensity and the calibrated vegetation indexes. We applied the support vector machine approach [18] to conduct a supervised classification of the reflectance of all the detection points from each object. The 780-nm signal, which represents a traditional single-wavelength LiDAR, exhibited a classification accuracy of only 55.9% [see Fig. 6(a)].

Classification was performed to demonstrate the discrimination capability of the vegetation indexes [see Fig. 6(b)–(d)]. The total classification accuracy of the three vegetation indexes were all above 90%. Therefore, the vegetation indexes that use different wavelengths are more effective than the traditional single wavelength in distinguishing various objects.

V. CONCLUSION

This letter has presented a wavelength-dependent LiDAR backscatter intensity calibration method that maximizes the advantages of multispectral LiDAR. We established a spectral ratio calibration method for multispectral LiDAR and investigated the effective calibration procedure for the mixed measurement of effects of incidence angle and surface roughness. The LiDAR spectral ratio was insensitive to sensor factors and advantageous in calibrating the effect of a known sensor inclination angle and the effect of a typically unknown target inclination with respect to the sensor. Moreover, the vegetation indexes produced by the LiDAR calibration procedure improved the classification accuracy.

Most calibration methods for LiDAR detection consider only a single wavelength. The development of the spectral ratio

method improves the calibration procedure of multispectral LiDAR. With the development of the multispectral LiDAR system, the approach should be further tested, and additional calibration factors should be considered. Therefore, this study can be regarded as a practical solution to the calibration problem of multispectral LiDAR.

REFERENCES

- [1] F. Morsdorf *et al.*, “Discrimination of vegetation strata in a multi-layered Mediterranean forest ecosystem using height and intensity information derived from airborne laser scanning,” *Remote Sens. Environ.*, vol. 114, no. 7, pp. 1403–1415, Jul. 2010.
- [2] C. Hopkinson and L. Chasmer, “Testing LiDAR models of fractional cover across multiple forest ecozones,” *Remote Sens. Environ.*, vol. 113, no. 1, pp. 275–288, Jan. 2009.
- [3] I. H. Woodhouse *et al.*, “A multispectral canopy LiDAR demonstrator project,” *IEEE Geosci. Remote Sens. Lett.*, vol. 8, no. 5, pp. 839–843, Sep. 2011.
- [4] T. Hakala, J. Suomalainen, S. Kaasalainen, and Y. Chen, “Full waveform hyperspectral LiDAR for terrestrial laser scanning,” *Opt. exp.*, vol. 20, no. 7, pp. 7119–7127, Mar. 2012.
- [5] G. Wei *et al.*, “Multi-wavelength canopy LiDAR for remote sensing of vegetation: Design and system performance,” *ISPRS J. Photogramm. Remote Sens.*, vol. 69, pp. 1–9, Apr. 2012.
- [6] W. Wagner, “Radiometric calibration of small-footprint full-waveform airborne laser scanner measurements: Basic physical concepts,” *ISPRS J. Photogramm. Remote Sens.*, vol. 65, no. 6, pp. 505–513, Nov. 2010.
- [7] B. Höfle, and N. Pfeifer, “Correction of laser scanning intensity data: Data and model-driven approaches,” *ISPRS J. Photogramm. Remote Sens.*, vol. 62, no. 6, pp. 415–433, Dec. 2007.
- [8] S. Kaasalainen *et al.*, “Radiometric calibration of LIDAR intensity with commercially available reference targets,” *IEEE Trans. Geosci. Remote Sens.*, vol. 47, no. 2, pp. 588–598, Feb. 2009.
- [9] A. Pesci and G. Teza, “Effects of surface irregularities on intensity data from laser scanning: An experimental approach,” *Ann. Geophys.*, vol. 51, no. 5–6, pp. 839–848, 2008.
- [10] M. A. Balduzzi, D. Van der Zande, J. Stuckens, W. W. Verstraeten, and P. Coppin, “The properties of terrestrial laser system intensity for measuring leaf geometries: A case study with conference pear trees (*Pyrus Communis*),” *Sensors*, vol. 11, no. 2, pp. 1657–1681, 2011.
- [11] S. Kaasalainen, A. Jaakkola, M. Kaasalainen, A. Krooks, and A. Kukko, “Analysis of incidence angle and distance effects on terrestrial laser scanner intensity: Search for correction methods,” *Remote Sens.*, vol. 3, no. 10, pp. 2207–2221, 2011.
- [12] S. Song, W. Gong, B. Zhu, and X. Huang, “Wavelength selection and spectral discrimination for paddy rice, with laboratory measurements of hyperspectral leaf reflectance,” *ISPRS J. Photogramm. Remote Sens.*, vol. 66, no. 5, pp. 672–682, Sep. 2011.
- [13] R. Gaulton, F. Danson, F. Ramirez, and O. Gunawan, “The potential of dual-wavelength laser scanning for estimating vegetation moisture content,” *Remote Sens. Environ.*, vol. 132, pp. 32–39, May 2013.
- [14] C. J. Tucker, “Red and photographic infrared linear combinations for monitoring vegetation,” *Remote Sens. Environ.*, vol. 8, no. 2, pp. 127–150, May 1979.
- [15] O. Nevalainen *et al.*, “Fast and nondestructive method for leaf level chlorophyll estimation using hyperspectral LiDAR,” *Agricult. Forest Meteorol.*, vol. 198, pp. 250–258, Nov./Dec. 2014.
- [16] A. A. Gitelson, Y. J. Kaufman, and M. N. Merzlyak, “Use of a green channel in remote sensing of global vegetation from EOS-MODIS,” *Remote Sens. Environ.*, vol. 58, no. 3, pp. 289–298, Dec. 1996.
- [17] E. W. Chappelle, M. S. Kim, and J. E. McMurtrey, III, “Ratio analysis of reflectance spectra (RARS): An algorithm for the remote estimation of the concentrations of chlorophyll a, chlorophyll b, and carotenoids in soybean leaves,” *Remote Sens. Environ.*, vol. 39, no. 3, pp. 239–247, Mar. 1992.
- [18] Y. Ma, and W. Gong, “Evaluating the performance of SVM in dust aerosol discrimination and testing its ability in an extended area,” *IEEE J. Sel. Topics Appl. Earth Observ. Remote Sens.*, vol. 5, no. 6, pp. 1849–1858, Dec. 2012.